

# Polymorphic Structures and Characteristics of Nematic-Based Ferronematics

Hiroya Nishikawa<sup>1</sup>, Fumito Araoka<sup>1</sup>

Hiroya.nishikawa@riken.jp

<sup>1</sup>RIKEN Center for Emergent Matter Science (CEMS)

Keywords: ferronematic, gigantic polarization, dielectric, ferroelectric, liquid crystal

## ABSTRACT

Recently, a new nematic polymorph with highly polar order has been found. This is just the long-awaited ferronematic ( $N_F$ ) phase. A common significant characteristic is a colossal dielectric permittivity ( $>10,000$ ) in the  $N_F$  phase. Here, the polymorphic structures and characteristics of a 1,3-dioxane-tethered ferronematogen (DIO) are introduced.

## 1 Introduction

The primordial nematic liquid crystal (NLC) has truly three-dimensional fluidity because of nematogens exhibit only orientational but no positional order. The unique electro-optical effect in NLCs has led the portable computing revolution of the 20th century in the liquid crystal display technologies. By contrast, a ferronematic ( $N_F$ ) LC, in which the local nematic director is non-degenerate, is of great fundamental and practical interest. Since prediction on  $N_F$  phase by Debye and Born 100 years ago, although an experimental evidence on the presence of  $N_F$  phase in some polymer liquid crystals, in low molecular mass materials it has unrevealed. However, more recently, the long-awaited  $N_F$  phase has been found in archetypal molecules, RM734 [1] and DIO [2] which would usher in an entirely new era in the history of liquid crystals. Common significant characteristics of them are ferroelectric response and a colossal dielectric permittivity ( $>10,000$ ) in the  $N_F$  phase. [2,3] Needless to say, they have vast potential for innovative applications by the proactive use of its gigantic dielectric properties. We would like to introduce unique properties, in particular, a new class of helical structure and a photo-variable capacitor based on a ferronematogen bearing a 1,3-dioxane unit in the mesogenic core (DIO) on the day. In this manuscript, we highlight the former topic, an electro-optic (EO) properties of the chiral ferronematic ( $N_F^*$ ) phase.[4]

## 2 Experiments

A host ferronematogen, DIO, was synthesized in our laboratory. A guest chiral dopant, (S)-ring3 (1) (from prof. Y. Ito, University of Tokyo) was employed. The LC blends, 1/DIO, was prepared by dissolving in chloroform followed by evaporation at 40 °C. Unless otherwise noted, we used a temperature controller and a hot stage (mK2000, INSTEC) to accurately control temperature of the LC sample. For each experiment with an applied  $E$ -field, we

used different system built by a waveform generator, a high-speed power amplifier and/or an oscilloscope. For POM and dielectric relaxation (DR) studies, we employed, respectively, two types of a sandwiched ITO glass cell: 1) homogeneous cell (inner glass surfaces are coated with PI and rubbed unidirectionally to yield a unidirectional homogeneous orientation, E.H.C., Japan, thickness: 5  $\mu\text{m}$ ) and 2) homeotropic cell (inner glass surfaces were coated with octadecyltriethoxysilane, handmade, thickness: 13.4  $\mu\text{m}$ , electrode area: 50  $\text{mm}^2$ ). We also used an in-plane system (IPS) cell (consists comb-like ITO electrodes, width: 10  $\mu\text{m}$ , gap: 10  $\mu\text{m}$ , thickness: 5  $\mu\text{m}$ , E.H.C., Japan) for POM, transmittance spectra as well as SHG studies. The DR studies was carried out during cooling at frequencies ranging between 1 Hz and 1 MHz using an impedance/gain-phase analyzer and a dielectric interface. The transmittance spectra were recorded using a fiber optic spectrometer and a UV/Vis/NIR spectrophotometer. The SHG investigation was carried out using a Q-switched Nd: YAG laser at  $\lambda = 1064$  nm with a 5 ns pulse width (pulse energy: 400  $\mu\text{J}$ ) and a 10 kHz repetition rate.

## 3 Results and Discussion

Figure 1 shows a comparison of the  $N^*$  and  $N_F^*$  structures confined between two rubbed substrates with planar anchoring. In the conventional  $N^*$  phase, there is a helicoidal structure in which the nematic director is twisted continuously at a certain pitch (Figure 1a). In this case, the structural periodicity in the helix direction corresponds to a half pitch of the helix due to the head-and-tail symmetry of the nematic director. Because of this half-pitch periodicity, the  $N^*$  phase is well known to exhibit optical reflection centered at the wavelength  $\lambda$ , which satisfies Bragg's condition for what is referred to as a half-pitch band (HPB),

$$m\lambda = 2n(p/2)\cos\theta = np\cos\theta, \quad (1)$$

where  $m$ ,  $n$ ,  $p$ , and  $\theta$  are the order of reflection, average refractive index, helical pitch, and incident angle of light, respectively. By contrast, in the  $N_F^*$  phase, both the nematic director and polarization are twisted together along the helical axis (Figure 1c). In other words, the local nematic director is non-degenerated, and the head-and-tail symmetry is broken, offering the periodicity of the system corresponds to a full pitch (FP). Thus, some

properties are expected to be altered in the  $N_F^*$  phase because of this non-degeneracy and polar property, as will be demonstrated in the following.

To characterize an induced chiral nematic ( $N^*$ ) and chiral ferronematic ( $N_F^*$ ) phases, the phase transition of 1/DIO was investigated by POM and DSC studies. The DSC result of 1/DIO (4 wt%) presented distinct exothermal peaks at 152 °C and 44.7 °C due to Iso- $N^*$  and  $N^*$ - $N_F^*$  phase transitions. The POM image of  $N^*$  phase (100 °C) presented a planar texture with a uniform birefringence color. Below 44 °C, a similar planar texture with slightly different color appeared. We also measured the SAX diffractograms of 1/DIO (4 wt%) in the  $N^*$  and  $N_F^*$  phases (not shown here). For the  $N^*$  (80 °C) and  $N_F^*$  phase (40 °C), one diffuse scattering was observed at  $2\theta = 22.4^\circ$ , and the corresponding  $d$ -spacing was calculated to be 0.40 nm. This halo is due to the mean distance of aromatic cores of molecules *e.g.* face-to-face or edge-to-face  $\pi$ - $\pi$  stacking. The helical structure throughout the  $N^*$  to  $N_F^*$  phase in our system was investigated using very common techniques for pitch estimation, *i.e.*, transmission spectra measurement and the Grandjean-Cano method. At 100 °C, the reflection band of 1/DIO (4 wt%) appeared at *ca.* 670 nm, corresponding to the HP period of the helix. With decreasing temperature, the center wavelength shifted to 640 nm at 39 °C (**Figure 2a**). The reflection band of the  $N_F^*$  phase at 39 °C was slightly broader than that of the  $N^*$  phase at 100 °C. Besides, the helical pitch of 1/DIO (2 wt%) was also estimated using the Grandjean-Cano method for a wedge cell. For the latter, we used the following equation:

$$p = 2L \tan \theta. \quad (2)$$

, where  $p$ ,  $L$ ,  $\theta$  are the helical pitch, distance across the Grandjean steps, and wedge angle, respectively. The helical pitches of  $N^*$  and  $N_F^*$  were almost similar, which was estimated from transmission spectra (**Figure 2b**), whereas the helical pitch changed discontinuously via the  $N^*$ - $N_F^*$  phase transition point (**Figure 2c**).

Let us discuss these significant discrepancies based on a possible model of the correct helical structure of the  $N_F^*$  phase. In the  $N^*$  phase, an integer multiple of the HP is confined in the wedge cell, and thus inevitable defect lines (so-called Cano lines), emerge between the mismatched helices (**Figure 2d,e**). By contrast, in the  $N_F^*$  phase, the direction of polarization should be considered for each helix because head-and-tail symmetry is broken. In this case, the uniformly aligned molecules at the substrate surface exhibited unidirectional polarization. The polarization rotates with the nematic director around the helical axis, but the surface polarization should match over the entire surface (**Figure 2h**). Consequently, only the even multiples of the HP are allowed so that the step width should be doubled (**Figure 2d,f,g**). In this case, the helical pitch of the  $N_F^*$  phase is calculated by the corrected equation as follows:

$$p = L \tan \theta. \quad (3)$$

Thus, the given correct pitch of the  $N_F^*$  phase was 0.85  $\mu\text{m}$ , which agrees well with the pitch of the  $N^*$  phase.

To confirm that a polar order exists in the  $N_F^*$  phase, we took place dielectric relaxation (DR) spectroscopy and second harmonic generation (SHG) studies (data set are not shown here). In the  $N^*$  phase, the dielectric permittivity ( $\epsilon'$ ) was  $\approx 20$  ( $f = 1$  kHz) at 100 °C, which gradually increased as a decrease of temperature. Further cooling allowed a phase transition from the  $N^*$  to the  $N_F^*$  phase. At the  $N$ - $N_F^*$  phase transition, the magnitude of  $\epsilon'$  jumped to 6500 ( $f = 1$  kHz). Note that the  $N$  and  $N_F$  phases in pure DIO display dielectric permittivity of a few hundreds and  $\approx 10000$ , respectively. Thus, it suggests that the  $N^*$  and  $N_F^*$  phases inherit the dielectric characteristics of the original  $N$  and  $N_F$  phases in the pure DIO. On the other hand, SHG signals of 1/DIO (4 wt%) were detected in the IPS cell with/without an application of  $E$ -field because SHG is a powerful tool for probing polar order in materials with noncentrosymmetric structures. Over the entire temperature range of the  $N^*$  phase, SHG was inactive irrespective of  $E$ -field application, indicating no polar ordering. However, non-zero SHG signal is observed and increased under the  $E$ -field in the  $N_F^*$  phase. When the  $E$ -field was removed, SHG intensity decreased to the original signal level immediately. The switching of SHG activity in the  $N_F^*$  phase was repeatable.

To investigate  $E$ -field-induced helix deformation, we performed the transmission spectroscopy of 1/DIO (4 wt%) injected in a PI-coated IPS cell. In the  $N^*$  phase (100 °C), the  $E$ -field (square-wave,  $2.0 V_{pp} \mu\text{m}^{-1}$ ,  $f = 100$  Hz) broadened the reflection band ( $\lambda = 680$  nm) and decreased the transmittance level by  $\approx 20\%$  (**Figure 3a**). It is suggested that helix deformation broadened the band while reducing the transmittance level due to light scattering from focal conics or the electro-hydrodynamic effect. By contrast, the  $N_F^*$  phase (39 °C) demonstrated only a small shift in the reflection band ( $\lambda = 650$  nm) by the  $E$ -field (square wave,  $2.0 V_{pp} \mu\text{m}^{-1}$ ,  $f = 100$  Hz), whereas band broadening and transmittance change were scarcely observed. Instead, new distinct peaks appeared at  $\approx 1300$  and 445 nm under the  $E$ -field (**Figure 3b**).

Let us consider this unusual  $E$ -field response of the  $N_F^*$  phase in terms of the Bragg condition (Eq. 1). When the  $E$ -field is applied normal to the helical axis of the  $N^*$  phase, the pristine helix is distorted. If the substrate surfaces are anchoring-free, the helical pitch increases nonlinearly as the  $E$ -field increases until a critical value  $E_c$ . However, under the strong planar anchoring, the nematic director at each substrate surface is strongly pinned down. Thus, the helix is deformed while maintaining periodicity (**Figure 1b**), unless the distorted helix breaks down to reduce stress under a strong  $E$ -field.

In this case, the high-order reflection bands of HPB appear at  $\lambda = np/m$ , but these are in the ultraviolet region and are therefore not observable in the present setup. By contrast, the unwinding process of the  $N_F^*$  helix is totally different because of coupling between the spontaneous polarization and polarity of the  $E$ -field (**Figure 1d**). When a DC  $E$ -field is applied, the nematic director reorients according to the polarity of the  $E$ -field (in case e.g. left to right in the figure plane), but the helix does not allow to unwind again due to surface anchoring. In this case, regions denoted as Section-A in Figure xx may grow because of coupling between the polarization and the polarity of  $E$ -field. By contrast, the other regions (Section-B), are compressed and invaded by Section-A. Thus, the HPB reflection diminishes. Instead, the full-pitch band (FPB) reflection at  $\lambda = 2np$  and its high-order reflections appear corresponding to the Fourier components of the deformed helix. Since the wavelength of the induced reflection band ( $\lambda \approx 1300$  nm) under the  $E$ -field was more or less twice that under the zero  $E$ -field ( $\lambda \approx 630$  nm), this new reflection band corresponds to FPB. The central wavelengths of the second and third bands are estimated to be 651 and 434 nm, respectively, which coincide with the experimentally obtained wavelengths ( $\lambda_{\text{obs}} = 656$  and 447 nm, 656 nm overlaps with HPB). This model was further supported by computational simulations based on the Berreman 4×4 matrix method (not shown here). Worth noting, an electric stimulus to the  $N_F^*$  phase enables selective switching between the HPB and FPB (+ higher order) modes under extremely low  $E$ -fields ( $< 2.0 V_{\text{pp}} \mu\text{m}^{-1}$ ). As mention above, the conventional  $N^*$  phase requires an extremely high operating voltage to generate higher-order reflection bands and cannot realize such switching between HPB and FPB. Thus, the EO behavior of the  $N_F^*$  phase may provide a feature distinct from the  $N^*$  phase and adds a new type of photonic band gap (PBG) switching.

Finally, the EO response based on the unique PBG switching was investigated. Here, we examined the temporal variation of the normalized transmittance  $T$  at 450 nm, for which a blue diode laser is available. Under the zero  $E$ -field, the beam could pass through the cell while maintaining its initial intensity, because the reflection band at 450 nm was not yet induced, *i.e.*,  $T = 100\%$ . By contrast, when an  $E$ -field (square-wave  $E$ -field packets,  $f = 100$  Hz,  $2.0 V_{\text{pp}} \mu\text{m}^{-1}$ ) was applied, the transmittance level was significantly reduced by 20–30% per step (**Figure 3c**). When the  $E$ -field was removed, the transmittance was restored to  $T = 100\%$ . We also estimated the EO response times during the reversible change of transmittance. The approximate estimates of ON/OFF response time,  $T_{\text{ON}}$  and  $T_{\text{OFF}}$  were, respectively, 250  $\mu\text{s}$  and 263  $\mu\text{s}$ , which were so similar values. As a similar helix-based EO switching, the vertically-aligned deformed-helix (VADH) mode that uses SmC\* FLC is a well-known approach for achieving a quick

response assisted by its twist elasticity. In this mode, the response time of this mode,  $T_{\text{ON}} = T_{\text{OFF}}$ , which are also defined as follows:

$$\tau = \eta / (Kq^2 + P_s E) \quad (4)$$

, where  $\eta$ ,  $K$ ,  $q$ ,  $P_s$  and  $E$  are the rotational viscosity, the twist elastic constant, the wavenumber of the helix, the spontaneous polarization and  $E$ -field, respectively. Because the configuration of VADH-FLC and our system are similar, Eq. 4 is adaptable to the present system. However, obtained ON/OFF response time are seems to be underestimated because the applied  $E$ -field is not uniform in our cell, which causes structural non-uniformity in the cell. Recently, Yamamoto et al. significantly reduced the  $T_{\text{OFF}}$  of VADH-FLCs down to ca. 20  $\mu\text{s}$  by utilizing an instantaneous reverse pulse field. This reverse pulse method would be also useful in the  $N_F^*$  phase because of its inherent polar structure. As expected,  $T_{\text{OFF}}$  was dramatically and successfully reduced to be 15  $\mu\text{s}$  (**Figure 3d**), which is remarkably faster than in conventional FLCs (surface-stabilized FLC, VADH-FLC) and others.

#### 4 Conclusion

In conclusion, we realized, for the first time, a new class of chiral nematic phase with helical polar order, *i.e.* chiral ferronematic phase ( $N_F^*$ ) by mixing a ferronematogen (DIO) with a chiral dopant ((S)-ring3). We proposed the polar helical structure in the  $N_F^*$  phase, in which the nematic director and spontaneous polarization are continuously twisted. Additionally, the dielectric and SHG studies clarified the presence of the large polar response was detected in the  $N_F^*$  phase which was distinct from the conventional  $N^*$  phase because of the non-degeneracy of the local nematic director, as observed in the fundamental optical behaviors in wedge cells or under  $E$ -fields. Especially, an electrically interconvertible selective reflection was related to the half-/full-pitch bands in the distorted helix in the  $N_F^*$  phase. In the  $N_F^*$  phase, the full-pitch band and higher-order modes were completely interchanged under low-voltage driving ( $1.6 V_{\text{pp}} \mu\text{m}^{-1}$ ). Such a mode-compatibility requires a significant high voltage for the conventional  $N^*$  phase. Moreover, we found the transmission level of  $N_F^*$ LC responded with an ultra-fast response time ( $\approx 15 \mu\text{s}$ ). These low-voltage driving and the ultra-fast EO response of  $N_F^*$ LC surpass those of the SmC\*-based FLC modes and VADH-FLCs. Through these investigations on the EO process, we determine that the  $N_F^*$  phase has a huge potential for application.

#### References

- [1] R. J. Mandle, S. J. Cowling and J. W. Goodby, "Rational Design of Rod-Like Liquid Crystals Exhibiting Two Nematic Phases", *Chem. - Eur. J.*, 23, 14554 (2017); R. J. Mandle, S. J. Cowling and J. W. Goodby, "A nematic to nematic transformation exhibited by a rod-like liquid crystal", *Phys. Chem.*

Chem. Phys., 19, 11429 (2017).

- [2] H. Nishikawa, K. Shiroshita, Y. Okumura, Y. Haseba, S. Yamamoto, K. Sago and H. Kikuchi, "A fluid liquid-crystal material with highly polar order," *Adv. Mater.*, 29, 1702354 (2017).
- [3] X. Chen, E. Korblova, D. Dong, X. Wei, R. Shao, L. Radzihovsky, M. A. Glaser, J. E. MacLennan, D. Bedrov, D. M. Walba and N. A. Clark, "First-principles experimental demonstration of ferroelectricity in a thermotropic nematic liquid crystal: Polar domains and striking electro-optics", *PNAS*, 117, 14021 (2020); X. Chen, E. Korblova, M. A. Glaser, J. E. MacLennan, D. Bedrov, D. M. Walba and N. A. Clark, "Polar in-plane surface orientation of a ferroelectric nematic liquid crystal: Polar monodomains and twisted state electro-optics" *PNAS*, 118, e2104092118 (2021).
- [4] H. Nishikawa and F. Araoka, "A new class of chiral nematic phase with helical polar order," *Adv. Mater.*, DOI: 10.1002/adma.202101305 (2021).

### Acknowledgement

We are also grateful to Y. Ito (University of Tokyo) for the chiral dopant, (S)-ring3 (**1**) and thank Mr. D. Morishita (University of Tokyo) for helping the XRD measurements. This work was financially supported by JST CREST, Grant Number JPMJCR17N1, Japan. This work was partially supported by JSPS KAKENHI Grant Number JP50835519 and 21H01801 from the Japan Society for the Promotion of Science (JSPS).

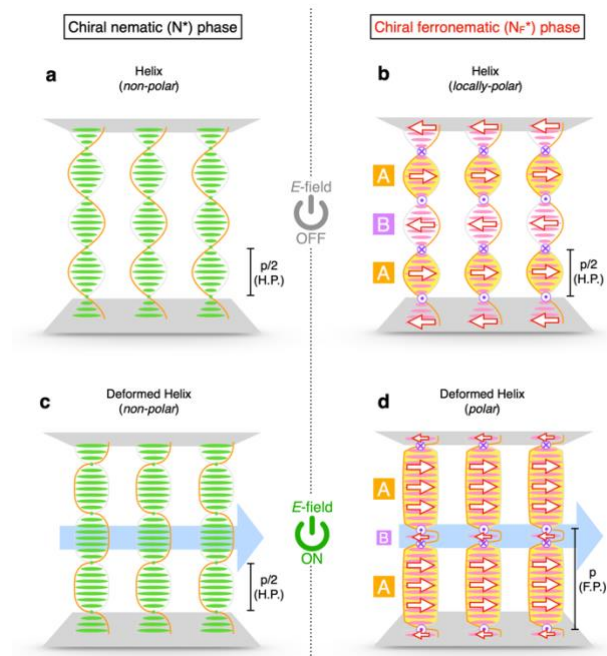


**Fig. 1** Schematic illustration of helical superstructures for chiral nematic ( $N^*$ ) (a,b) and chiral ferronematic ( $N_F^*$ ) phases (c,d). (adapted from ref.4, with permission from Wiley-VCH, 2021)

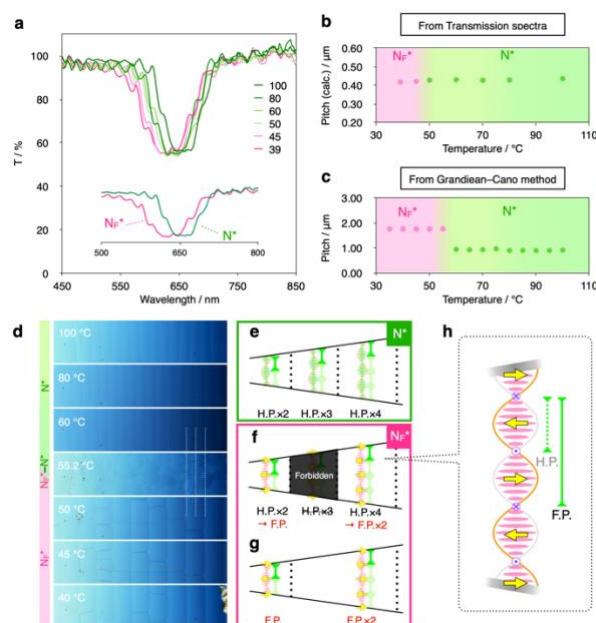


**Fig. 2** Helical pitch analysis of  $N^*$  and  $N_F^*$  phases for 1/DIO. a) Transmission spectra in various temperature. Helical pitch vs. temperature estimated from transmission spectra (b) and from Cano method (c). d) Textural changes in Grandjean steps. e–g) Schematic illustrations of  $N^*$  and  $N_F^*$  helices confined in wedge cell. (adapted from ref.4, with permission from Wiley-VCH, 2021)

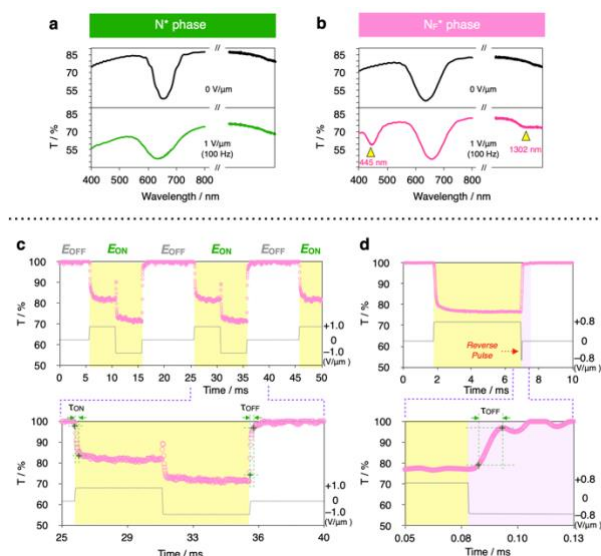


**Fig. 3** EO properties of  $N^*$  and  $N_F^*$  phases. a, b) UV-Vis spectra changing with/without  $E$ -field for  $N^*$  (a) and  $N_F^*$  phase (b). c) ON/OFF behavior of transmission level at 450 nm with/without  $E$ -field. d) Accelerated turn-off response with aid of additional reverse pulse. Conditions:  $E$ -field (square wave,  $E = 1.6$  or  $2.0$  Vpp  $\mu\text{m}^{-1}$ ,  $f = 100$  Hz). (adapted from ref.4, with permission from Wiley-VCH, 2021)